

# Bipedal walking of an octopus-inspired robot

Marcello Calisti, Francesco Corucci, Andrea Arienti, and Cecilia Laschi

The BioRobotics Institute, Scuola Superiore Sant'Anna, Pisa, Italy,  
m.calisti@sssup.it

**Abstract.** In this paper a model is presented which describes an octopus-inspired robot capable of two kinds of locomotion: crawling and bipedal walking. Focus will be placed on the latter type of locomotion to demonstrate, through model simulations and experimental trials, that the robot's speed increases by about 3 times compared to crawling. This finding is coherent with the performances of the biological counterpart when adopting this gait. Specific features of underwater legged locomotion are then derived from the model, which prompt the possibility of controlling locomotion by using simple control and by exploiting slight morphological adaptations.

**Keywords:** bio-inspired robotics, underwater locomotion, embodied intelligence

## 1 Introduction

Legged robotics is the branch of robotics studying the static, quasi-static and dynamic locomotion of robots that move using limbs [1]. Legged locomotion has significant advantages compared to other types of locomotion, e.g. it reduces damages to the environment and is particularly suited for uneven terrains [2].

The investigation of the neural, bio-mechanical and mathematical aspects of legged locomotion, has led computer scientists and engineers to infer a close relationship between locomotion and intelligence [3]. At the same time, biologists and mathematicians have focused their work on basic walking and running models, called templates [4], which describe the locomotion of animals and robots with an arbitrary number of legs [5]. These synergistic efforts among different specializations have brought significant scientific [6] and technological [7] results, with potential for the development of ever more effective and efficient artificial machines.

Despite the vast amount of studies on the subject, there is still a niche that requires further investigation: underwater legged locomotion (ULL). While some biologists analyze aquatic animal walking and running [8], few robotic researchers work in this niche. Marine robotics involves mainly the study of swimming systems, such as remotely operated vehicles (ROVs) or autonomous underwater vehicles (AUVs), or more recently bioinspired fish [9] or cephalopods [10]. These robots usually work near submersed structures; they need to be accurately controlled to avoid damages to fragile surfaces or to the robot itself. Conversely,

legged robots require a substrate to move on and, as mentioned, they are able to prevent damages and move in unstructured environments. In this context, marine robotics could benefit from the progress made on legged robots, and a new generation of underwater legged robots (ULRs) could arise.

To the best of our knowledge, there are very few ULRs and they are still far from the successes of their terrestrial counterparts. Among them, one of the most advanced is called Crabster200 (CR200) [11], an hexapedal robot equipped with three degrees of freedom (DoF) limbs. Currently there are no reports either on the performances of CR200, or on its control strategies. Another related platform is a bio-inspired robot featuring elastic limbs, developed by the author [12]. By synthesizing mechanical [13] and control [14, 15] aspects, the robot mimics the crawling locomotion of the *Octopus vulgaris*. With a pushing-based locomotion strategy the robot moves omnidirectionally, translating the center of mass (CoM) from one position to another in a quasi-static locomotion that alternates pushing phases and recovery phases. This kind of behavior represents one of the basic locomotion strategies of the octopus, which is, however, among the slowest performed by the animal [16].

The work presented here addresses another movement employed by the animal: bipedal walking. Bipedal walking differs from crawling mainly in two aspects. Firstly, when performing this kind of motion the octopus is not sprawled over the substrate, but floats a few centimeters from the ground. Secondly, bipedal walking is considerably faster than crawling. This kind of motion can be performed with a pair of arms pushing alternately or together [16]. With the aim to increase the performances of ULRs, this work investigates underwater bipedal walking. A model based on an extension of the bioinspired octopus-robot previously presented in [12] was developed here and simulations were compared with underwater trials performed by the actual robot. The validated model was then used to explore different morphological configurations of the robot and the resulting locomotion.

## 2 Robot and Model Description

A variety of models with different levels of complexity were developed to capture the dynamics of robot and animal locomotion. A seminal work is the spring loaded inverted pendulum (SLIP), a simple conservative spring-mass model for sagittal plane locomotion [17]. Despite its simplicity, the SLIP model describes the basic motions and ground reaction forces for a broad range of animals. More complex models exist which describe the locomotion of insects, animals or robots, with accuracy ranging from accurate reproduction of the muscular system [18] to simplified compliant massless legs [19, 20]. The model presented in this work comprises massless compliant legs, and introduces some original key components of underwater legged dynamics. It is based on the crawling robotic platform presented in [12], which is briefly recalled in Sect. 2.1 for the reader's convenience.

## 2.1 Robotic platform

The robot is made of a swimming, a crawling and a floating module, as shown in Fig. 1a. The swimming module is not actuated in this experimentation, thus completely passive. The crawling module, based on the three-bar mechanism implemented by the authors in [12], comprises four compliant legs radially distributed with respect to a central body. The floating module is oriented  $(b, \beta)$  toward the rear side of the robot, modifying the resting posture from the sprawled posture used for crawling to one that is more suitable for bipedal locomotion (Fig. 1b) and similar to the one assumed by the octopus. The parameter  $b$  is the distance between the center of buoyancy (CoB) and CoM, while  $\beta$  represents the orientation of the CoB with respect to the vertical. The floating module can be inflated and deflated, thus varying the robot mean density  $\rho_r$ . Due to the posture obtained passively thanks to the floating module, only the frontal legs were activated in the present experiment.

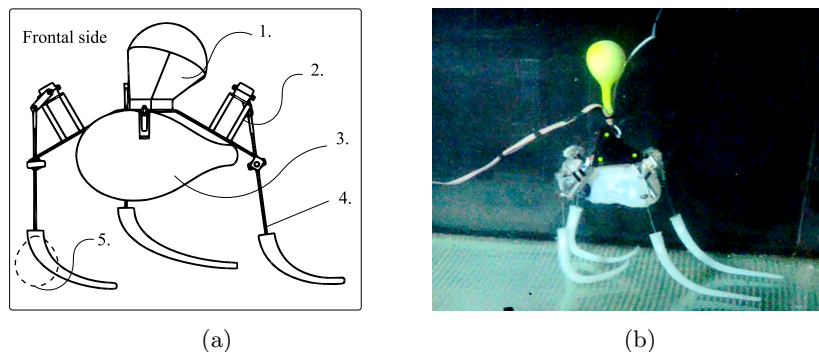


Fig. 1: The designed robot (a) and its mechanical components: 1. floating module, 2. leg mechanism, 3. swimming module and 4. compliant limb. The dashed line 5. identifies the end effector trajectory. The actual robot while moving inside the working space (b).

## 2.2 Model description

The sagittal plane model, with geometrical parameters selected to match the actual robot, comprises a central body with three DoF and four legs, immersed in water (Fig. 2). Reaction forces are applied to the CoM, while the buoyancy force is applied to the CoB. Legs are approximated as massless spring-damper systems and their kinematics are derived from the mechanism described in [12]. The distal parts of the legs, made of silicone, were neglected. The parameters and variables of the model are summarized in Table 1. The state variable  $\vartheta_l$  is explicitly considered simply for convenience, however it depends on  $\vartheta_m$  as

follows:

$$\vartheta_l = 2\pi - \arctan\left(\frac{m \cdot \sin(\vartheta_m + \alpha)}{i - m \cdot \cos(\vartheta_m + \alpha)}\right) - \vartheta_m - \alpha \quad (1)$$

Table 1: Parameters and variables of the proposed model

State variables		Geometric parameters	
$\vartheta_r$	pitch of the robot	$m$	length of the crank
$\vartheta_m$	angle of crank rotation	$l$	length of the arm
$\vartheta_l$	angle of leg rotation	$d$	distance between the crank's two CoRs
$x_g$	absciss coordinate of the CoM	$i$	distance from crank's CoR to bearing
$y_g$	ordinate coordinate of the CoM	$b$	distance from CoM to CoB
		$\alpha$	angle between $d$ and $i$
		$\beta$	angle between $b$ and medial plane
Dynamic parameters			
$k$	stiffness of the leg	$M$	mass of the robot
$c_{da}$	damping coefficient of the leg	$\bar{J}$	aggregate inertia of the robot
$c_{dr}$	drag coefficient	$V$	volume of the robot
$X_{uu}$	aggregate drag coefficient	$\rho_w$	density of the water
$c_{df}$	dynamic friction coefficient	$\rho_r$	mean density of the robot
$c_{sf}$	static friction coefficient	$g$	gravity acceleration
$\bar{M}$	mass of the robot + added mass		

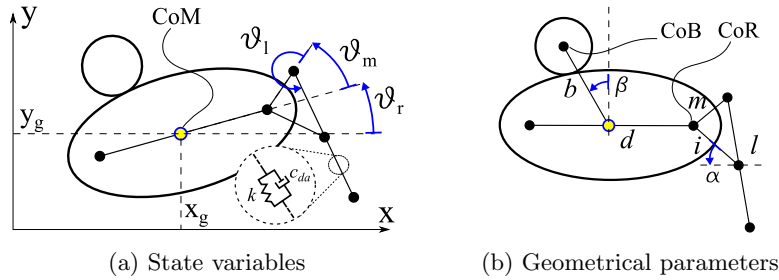


Fig. 2: Schemes of the robot model: only one frontal leg is shown. Dimensions are not proportional to those of the real robot.

By taking Fig. 2 as reference, it is possible to derive the kinematic equations of the legs. The positions of the frontal legs are reported in Eq. 2 and those of the rear legs are derived accordingly. Please note the following abbreviations:  $c_r \equiv \cos(\vartheta_r)$ ,  $c_{rm} \equiv \cos(\vartheta_r + \vartheta_m)$ , and so on for  $c_{rml}$ . The same convention is used for sines, i.e.  $s_r \equiv \sin(\vartheta_r)$  etc.

$$\mathbf{L} = \begin{bmatrix} x_g + \frac{d}{2}c_r & m \cdot c_{rm} & l \cdot c_{rml} \\ y_g + \frac{d}{2}s_r & m \cdot s_{rm} & l \cdot s_{rml} \end{bmatrix} \cdot \begin{bmatrix} 1 & 1 & 1 \\ 0 & 1 & 1 \\ 0 & 0 & 1 \end{bmatrix} \quad (2)$$

Given that the notation  $L_{ij}$  refers to the element  $(i, j)$  of the matrix  $\mathbf{L}$ ,  $L_{1j}$  in Eq.2 identifies the  $x$  position of joint  $j$ , while  $L_{2j}$  identifies the  $y$  position of joint  $j$ . Joint speeds are obtained by analytical derivation of Eq.2, and are identified with the same convention as  $S_{ij}$  (this time with respect to the matrix  $\mathbf{S}$ ). Since each leg is considered as a spring-damper system, starting from their positions and speeds, it is possible to derive the forces exerted by the legs to the ground, specifically elastic and damping forces. A touch-down vector  $\mathbf{t}$  is used as an auxiliary vector to identify whether the leg is in contact with the ground, i.e. if the condition  $L_{23} < 0$  is verified or not. The  $x$  position of the touch-down is stored in  $x_t$ , and the current length of the leg is derived as  $A = \sqrt{L_{22}^2 + (x_t - L_{21})^2}$ . Compressions in the  $x$  and  $y$  directions are, respectively (Eq. 3):

$$\begin{aligned} dL_x &= (x_t - L_{12}) \left( \frac{l}{A} - 1 \right) \\ dL_y &= L_{22} \left( \frac{l}{A} - 1 \right) \end{aligned} \quad (3)$$

The associated elastic forces are  $F_{el_x} = kdL_x$  and  $F_{el_y} = kdL_y$ . By taking the first derivative of the compressions (Eq. 3), the damping forces of the legs can be evaluated, being respectively  $F_{da_x} = c_{da}d\dot{L}_x$  and  $F_{da_y} = c_{da}d\dot{L}_y$ . In addition, gravity  $F_g = Mg$ , buoyancy  $F_b = \rho_w Vg$  and drag forces  $F_{dr_x} = \frac{1}{2}X_{uu}\dot{x}|\dot{x}|$ ,  $F_{dr_y} = \frac{1}{2}X_{uu}\dot{y}|\dot{y}|$  are applied to the body. The parameter  $X_{uu}$  is called aggregate drag coefficient as it combines information related to the drag coefficient and the reference area affecting the drag force.

Finally, the following equations describe the dynamics of the body (Eq. 4):

$$\begin{aligned} \overline{M}\ddot{x} &= \sum_{n=0}^4 t_n (F_{e_x} + F_{da_x})_n + F_{dr_x} \\ \overline{M}\ddot{y} &= \sum_{n=0}^4 t_n (F_{e_y} + F_{da_y})_n + F_{dr_y} + F_g + F_b \\ \overline{J}\ddot{\vartheta} &= \sum_{n=0}^4 t_n [(x_{t_n} - x_g)(F_{e_y} + F_{da_y})_n - y_g(F_{e_x} + F_{da_x})_n] + F_b \cdot b \cdot \sin(\vartheta) \end{aligned} \quad (4)$$

The quantity  $\overline{J}$  in Eq. 4 is called aggregate inertia coefficient as it embeds the body inertia plus the added inertia of the robot. It is not unusual that a leg slips on the ground, thus a slipping condition is checked at each instant. When the slipping condition  $|F_{e_x} + F_{da_x}| > c_{sf}(F_{e_y} + F_{da_y})$  is verified, the force exerted by the leg to the ground is considered  $c_{df}(F_{e_y} + F_{da_y}) \frac{S_{i3}}{|S_{i3}|}$  as described in [18]. The position of the touch-down  $x_t$  is updated by calculating the new positions  $L_{13}$  and verifying the touch-down condition  $L_{23} < 0$ .

### 3 Experimental methods

Motion kinematics were derived and used to estimate the unknown parameters of the model by recording the robot while it moved inside a tank. After estimating the parameters, a number of geometrical properties of the model were varied and the resulting locomotion was studied in simulation.

#### 3.1 Robot bipedal trials

The robot (equipped with a plate with 3 LEDs) was recorded while moving in a tank with 8 markers that define the working space of the runs. A direct linear transform (DLT) with 11 parameters was used to reconstruct the 3-dimensional positions of the LEDs and accordingly derive the 3-dimensional coordinates of the CoM (the reconstruction procedure is described in detail in [12]).

The floating module was connected to a pneumatic system that was manually actuated; a desired density, i.e.  $\rho_r = 1238 \text{ Kg/m}^3$ , was heuristically selected and kept constant during each trial session, comprising of five to ten runs by the robot. Each leg is actuated by a GM12a DC motor, that was properly insulated from the water by an *ad hoc* scaffold. Motors were plugged to a 5V Kert stabilized power supply, and were manually activated by a remote controller. The leg cranks rotate together at a constant speed of about  $\dot{\vartheta}_m \simeq 12.57 \text{ rad/s}$ , thus a purely feed-forward control is adopted. Although a phase shift between the legs is achievable and could be interesting to explore, at the moment they are actuated in phase.

Four features were extracted from each run, which characterize the locomotion: amplitude ( $a$ ), mean value ( $\mu$ ), frequency ( $f$ ) of the  $y_g$  oscillation and mean speed in the  $x$  direction ( $s$ ). The CoM moved approximately onto the x-y plane, so velocity in the  $z$  direction was considered to be null. Feature extraction was performed considering the latter part of the test, when the robot achieved stable periodic orbit.

#### 3.2 Parameter estimation

In order to validate the model, a number of model parameters had to be specified. Geometrical parameters were measured and directly plugged into the model. As for the unknown parameters, a parameter estimation procedure was set up. The parameters relevant to the estimation procedure are listed in Table 2. The decision to identify some parameters as aggregate quantities ( $X_{uu}$ ,  $\bar{J}$ ) is motivated by the fact that some of the involved quantities are difficult to measure or to estimate individually. For example, the shape of the robot is complex and irregular: it is difficult, therefore, to estimate the reference area (that also changes dynamically) for computing drag forces. Similar considerations apply to the aggregate inertia coefficient  $\bar{J}$ . The problem was formulated as a bounded minimum optimization problem. The fitness function was defined in terms of a 4-dimensional fitness vector, extracted from the model simulations, enclosing the features mentioned in Sect. 3.1, i.e. amplitude ( $a$ ), frequency ( $f$ ), mean value

Table 2: Parameters to be estimated and their bounds. The coefficient  $dr$  is the damping ratio  $dr = c_{da}/2\sqrt{kM}$  and  $c_{dfmul} = c_{df}/c_{sf}$

$k$	$dr$	$c_{sf}$	$c_{dfmul}$	$\bar{M}$	$X_{uu}$	$\bar{J}$
[25, 400]	[0, 0.9]	[0.6, 0.9]	[0.6, 0.9]	[0.755, 7.55]	[0.11, 145]	$[2.7 \cdot 10^{-4}, 1.79 \cdot 10^{-2}]$

( $\mu$ ) of the oscillation of the CoM in the  $y$  axis, and mean speed ( $s$ ) in the  $x$  axis ( $fitnessVector = (a, f, s, \mu)$ ). A target vector ( $targetVector = (a^*, f^*, s^*, \mu^*)$ ) was extracted from the trial of the actual robot, and the fitness value was computed as the sum of normalized squared errors between target and fitness vectors.

In our setup, the optimization algorithm must have the ability to cope with discontinuous objective functions, in order to handle situations in which the behavior of a parameter set cannot be quantified. For example, in our simulations, when a set of parameters caused the robot to fall or produce unstable behavior, the fitness was set to NaN. This is usually a problem with gradient-based approaches. For this reason, genetic algorithms were selected as a suitable alternative, as they can simply not consider individuals with NaN fitness for selection and reproduction. Furthermore, they are capable of finding global solutions with no prior assumptions or information about the objective function.

Among the several variants of genetic algorithms, a real-coded version of the Augmented Lagrangian Genetic Algorithm (ALGA) [21] was adopted for its ability to handle bounds and constraints. As for genetic operators, adaptive feasible mutation and scattered crossover were used. Genetic optimization was performed on a population of 500 individuals, with chromosomes composed of 7 genes encoding the parameters to be estimated. Evolution could last for 1000 generations maximum, with additional stop conditions based on the change of average fitness and maximum execution time.

Bounds were defined by considering extreme limit cases of physical feasibility. As an example, the lower bound for the aggregate drag coefficient  $X_{uu}$  is the one of a streamlined body (a shape featuring very low drag coefficient) with a circular exposed surface having a radius of just 3 cm, while the upper bound is given by a short cylinder (a shape featuring very high drag coefficient) enclosing the entire robot.

### 3.3 Model simulations

The model was validated using the approach described in Sect. 3.2, with the following geometrical parameter values:  $m = 0.022$  m,  $l = 0.12$  m,  $d = 0.15$  m,  $i = 0.056$  m,  $b = 0.088$  m,  $\alpha = 82$  deg,  $\beta = 16$  deg. After validation, further simulations were performed varying only parameters  $b$  and  $\beta$ , which define the position of the CoB. The model was numerically solved using Matlab<sup>®</sup>.

## 4 Results

Despite the high compliance of the legs, the robot is not sprawled on the ground, as happens outside water, due to the buoyancy module and the low density materials composing the legs and the swimming module. Simple feed-forward activation was used to make the robot achieve forward locomotion at a mean speed of  $\bar{x} = 0.0411 \text{ m s}^{-1}$  with a standard deviation of  $\text{s.d.} = 0.0024$ . Even when all the parameters were kept constant during the various runs, the robot slightly changed its mean velocity due to small changes in the testing conditions, such as the deposition of material inside the tank that slightly changed the friction to the ground. During locomotion, the frontal legs pushed the body forward and generated a positive momentum that made the frontal part of the robot rise. On the other hand, the buoyancy module, since displaced from the resting position, generated a negative momentum that lowered the frontal part. The designed geometrical configuration of the robot, i.e. the selection of  $b$  and  $\beta$ , did not lead to any falls occurring during locomotion.

In order to estimate the parameters, the fastest trial was selected as target, with the extracted vector being  $(a^*, f^*, s^*, \mu^*) = (0.0044, 2, 0.045, 0.12)$ . The achieved fitness value was  $9.1647 \cdot 10^{-6}$  (Table 3), with the model closely matching the behavior of the robot. A comparison between the CoM track of the robot and the one of the model is presented in Fig. 3. The error has been computed as the mean absolute value of the difference between the two CoM tracks.

Table 3: Evolved genome: identified parameters for  $\rho_r = 1238$

$k$	$dr$	$c_{sf}$	$c_{dfmul}$	$\bar{M}$	$X_{uu}$	$\bar{J}$	Fitness
216.5	0.37	0.65	0.83	4.64	121	0.014	$9.1647 \cdot 10^{-6}$

Once the parameters were estimated, since the actual robot has a fixed geometrical structure, the model was used to investigate the dynamics of the system with respect to variations in the CoB position. Initial conditions and all parameters, apart from  $b$  and  $\beta$ , were kept fixed and the resulting locomotion was analyzed. Interestingly, a variety of stable locomotion patterns arose, with different characteristics and speed (Fig. 4). Variations in CoB position led to considerable differences in the resulting locomotion, with some robots proceeding forward and others backward, at different speeds. By taking as reference the configuration of the real robot (for which parameter estimation was performed), simulations highlighted that a variation of  $\Delta\beta = +8.8 \text{ deg}$ ,  $\Delta b = -0.009 \text{ m}$  causes an inversion of motion. Simulations also pointed out that, by changing the position of the CoB, enhanced performances can be achieved with respect to forward locomotion. A variation of  $\Delta\beta = +18.9 \text{ deg}$ ,  $\Delta b = 0.14 \text{ m}$  prompted a significant improvement in speed (by a factor of  $\sim 1.7$ ) with respect to that exhibited by the robot.

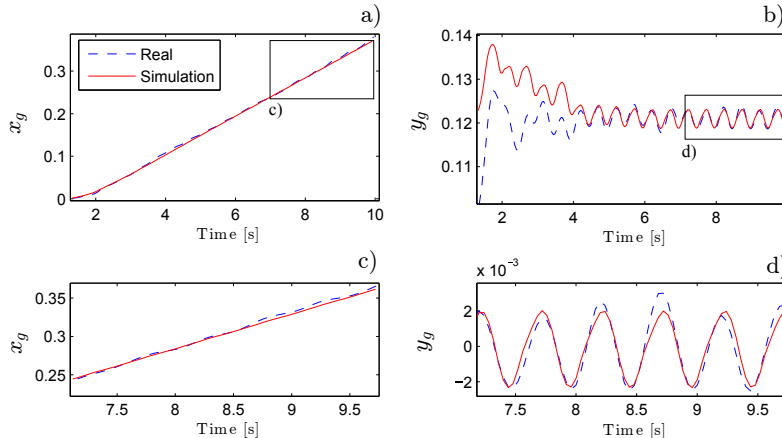


Fig. 3: Trajectories of  $x_g$  (a) and  $y_g$  (b) for the model executed with the estimated parameters. In c, d) the comparison of real and simulation data is highlighted. The displacement errors in  $y$  (meters) are: mean 0.0037, min  $1.6 \cdot 10^{-6}$  and max 0.02. The displacement errors in  $x$  (meters) are: mean 0.003, min 0.00014, max 0.0068.

## 5 Discussion

By keeping a bipedal body posture and using a feed-forward control, the robot's speed was higher than in crawling locomotion. This is coherent with the speed increase observed in the biological counterpart. Quantitatively, average speeds of octopuses are  $0.62 \text{ BL s}^{-1}$  and  $1.34 \text{ BL s}^{-1}$  respectively for crawling and bipedal walking [16] (BL stands for body lengths). Bipedal walking appears to be 2.16 times faster than crawling. Analogously, the robot's speed increases from  $1.52 \text{ cm s}^{-1}$  for crawling [12] to  $4.4 \text{ cm s}^{-1}$  for bipedal walking. The increase ratio is about 2.9, thus slightly higher for the robot than for the animal. This demonstrates the capability of this type of robot, i.e. a robot with elastic limbs, to perform both crawling and bipedal walking. The features of this kind of locomotion can be further analyzed by considering the results of the model simulations. The parameter estimation methodology proposed was effective despite the significant number of parameters, with small errors in fitness evaluation (Table 3) and a good match between real and simulated signals (Fig. 3).

Moreover, despite the wide bounds, the evolved parameters all look very plausible (Table 3). Notice that the hydrodynamics parameters,  $\bar{M}$ ,  $X_{uu}$  and  $\bar{J}$ , appear to provide a relevant contribution to the dynamics. As an example, in our case, the estimated added mass was  $\bar{M} \simeq 6M$  while ROV added masses usually range between 2-3 times the mass of the robot [22, 23]. The added mass value increases when there are irregular shapes and sharp transitions between the underwater vehicles' structure and the fluid, thus a higher value of  $\bar{M}$  than in traditional ROVs was expected. Moreover the proximity of the substrate en-

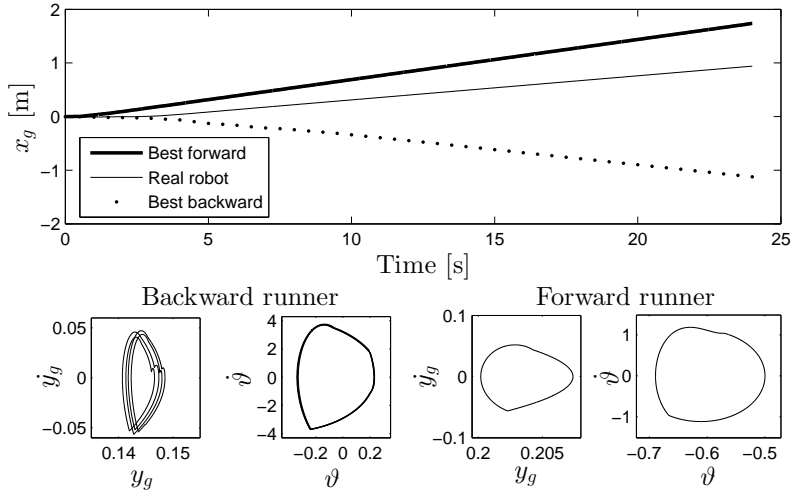


Fig. 4: By varying the position of the CoB ( $\beta$ ,  $b$ ) considerable differences are observed in the resulting locomotion. Top plot: Starting from the configuration of the real robot (middle curve) a variation of  $\Delta\beta = +8.8$  deg,  $\Delta b = -0.009$  m causes an inversion of motion (lower, dotted curve). A  $\Delta\beta = +18.9$  deg,  $\Delta b = 0.14$  m (upper, thick curve) entails instead a significant improvement in forward speed (by a factor of  $\sim 1.7$ ). There are several other trajectories between the plotted curves (not shown for readability). Bottom: stability of the best backward (left) and forward (right) runners. As for the backward runner, what may seem a still unstable orbit is instead a stable one, being composed of four cycles.

tails an additional increase, as known from potential flow analysis of bodies translating close to a fixed boundary [24]. Similar arguments stand for the other parameters, highlighting the difference between terrestrial legged locomotion and ULL.

Another peculiar aspect of ULL is the separation between the CoM and the CoB of the robot. This morphological trait implies, passively, the bipedal posture of the robot, leading to a significant speed increase in the presence of the same feed-forward control. This aspect was further explored through the proposed model, demonstrating that changes in CoB position can be exploited to achieve different locomotion patterns (backward or forward at different speeds). Given the stressed interaction with the environment, a small change in underwater robot morphology (i.e. CoB position) entails significant changes in the resulting behavior. This has a strong connection with the concept of embodied intelligence and morphological computation. Based upon the stable locomotion highlighted in Fig. 4, we envision the possibility to switch among different stable locomotion patterns by controlling slight morphological adaptations on-line and so allow smooth transition among stable orbits. Above all, the results we have presented

offer, for the first time, a starting point for the definition of quantitative design criteria for ULRs. As shown in Fig. 4, geometrical and morphological aspects can be properly designed to improve the robot's performances.

## 6 Conclusion

In this paper an octopus-inspired robot, capable of multi-gait locomotion, has been presented together with its model. It has been shown that the robot is able to perform bipedal locomotion, with a speed increase (with respect to crawling) that is consistent with biological observations. A model comprising massless spring legs has been proposed to describe the bipedal gait of the robot and has been validated against actual robot trials. The parameter estimation procedure, performed using genetic algorithms, highlighted the prominent role of hydrodynamics effects on the robot's dynamics. Furthermore, the model allowed a preliminary analysis of specific ULL features. The role of the CoB position was investigated, showing that it has a key role in determining the direction and speed of locomotion in the presence of the same feed-forward control, with potential implications on the embodied intelligence framework. This is a peculiar mechanism for ULL that is absent in terrestrial locomotion, where the role of the medium (i.e. air) is usually neglected. Presented methods and results also offer room for the exploration of optimal design for ULRs. By using evolutionary techniques to co-evolve both morphology and control, it is possible to take advantage of the significant body-environment interaction existing in underwater environments and to enhance the performances of ULRs.

## Acknowledgments

This work was supported in part by the Fondazione Livorno within the framework of the PoseiDRONE project Grant.

## References

1. Raibert, M.H.: Legged robots that balance. The MIT Press (1986)
2. de Santos, P., García, E., Estremera, J.: Quadrupedal locomotion: an introduction to the control of four-legged robots. Springer (2006)
3. Pfeifer, R., Iida, F., Gomez, G.: Morphological computation for adaptive behaviour and cognition. International Congress Series (1291) (2006) 22–29
4. Full, R., Koditschek, D.: Templates and anchors: neuromechanical hypotheses of legged locomotion on land. *The journal of experimental biology* **222** (1999) 3325–3332
5. Blickhan, R., Full, R.J.: Similarity in multilegged locomotion: bouncing like a monopode. *Journal of Comparative Physiology A* **173**(5) (1993) 509–517
6. Holmes, P., Full, R.J., Koditschek, D., Guckenheimer, J.: The dynamics of legged locomotion: Models, analyses, and challenges. *SIAM Review* **48**(2) (Jan 2006) 207–304

7. Saranli, U., Buehler, M., Koditschek, D.E.: Rhex: A simple and highly mobile hexapod robot. *International journal of robotics research* **20**(7) (2001) 616–631
8. Martinez, M.M.: Running in the surf: hydrodynamics of the shore crab *grapsus tenuicrustatus*. *The Journal of Experimental Biology* **204** (2001) 3097–3112
9. Zheng, C., Shataru, S., Xiaobo, T.: Modeling of biomimetic robotic fish propelled by an ionic polymer–metal composite caudal fin. *IEEE Transactions on Mechatronics* **15** (2010) 448–459
10. Serchi, F.G., Arienti, A., Laschi, C.: Biomimetic vortex propulsion: towards the new paradigm of soft unmanned underwater vehicles. *IEEE/ASME Transactions On Mechatronics* (2013) 1–10
11. Shim, H., Jun, B.H., Kang, H., Yoo, S., Lee, G.M., Lee, P.M.: Development of underwater robotic arm and leg for seabed robot, crabster200. In: *OCEANS - Bergen, 2013 MTS/IEEE*. (2013)
12. Calisti, M., Arienti, A., Renda, F., Levy, G., Mazzolai, B., Hochner, B., Laschi, C., Dario, P.: Design and development of a soft robot with crawling and grasping capabilities. In: *Proc. IEEE Int. Conf. Robotics and Automation, IEEE* (May 2012) 4950–4955
13. Calisti, M., Giorelli, M., Levy, G., Mazzolai, B., Hochner, B., Laschi, C., Dario, P.: An octopus-bioinspired solution to movement and manipulation for soft robots. *Bioinspiration & biomimetics* **6**(3) (2011) 036002
14. Li, T., Nakajima, K., Calisti, M., Laschi, C., Pfeifer, R.: Octopus-inspired sensorimotor control of a multi-arm soft robot. In: *IEEE Mechatronics and Automation, IEEE* (August 2012) 948–955
15. Calisti, M., Giorelli, M., Laschi, C.: A locomotion strategy for an octopus-bioinspired robot. In Prescott, T.J., Lepora, N.F., Mura, A., Verschure, P.F.M.J., eds.: *Living Machines. Volume 7375 of Lecture Notes in Computer Science.*, Springer (2012) 337–338
16. Huffard, C.: Locomotion by *abdoopus aculeatus* (cephalopoda: octopodidae): walking the line between primary and secondary defenses. *The J. of Experimental Biology* **209** (2006) 3697–3707
17. Blickhan, R.: The spring-mass model for running and hopping. *Journal of Biomechanics* **22**(11/12) (1989) 1217–1227
18. Iida, F., Rummel, J., Seyfarth, A.: Bipedal walking and running with spring-like biarticular muscles. *Journal of biomechanics* **21** (2008) 656–667
19. Ankarali, M.M., Saranli, U.: Control of underactuated planar pronking through an embedded spring–mass hopper template. *Auton Robot* **30** (2011) 217–231
20. Gerner, M., Albu-Schaffer, A.: A robust sagittal plane hexapedal running model with serial elastic actuation and simple periodic feedforward control. In: *IROS*. (2013)
21. Conn, A.R., Gould, N.I., Toint, P.: A globally convergent augmented lagrangian algorithm for optimization with general constraints and simple bounds. *SIAM Journal on Numerical Analysis* **28** (1991) 545–572
22. Caccia, M., Indiveri, G., Veruggio, G.: Modeling and identification of open-frame variable configuration unmanned underwater vehicles. *IEEE JOURNAL OF OCEANIC ENGINEERING* **25** (2000) 227–238
23. Ridaou, P., Battle, J., Carreras, M.: Model identification of a low-speed uuv. In Katebi, R., ed.: *IFAC PROCEEDINGS SERIES*. (2002) 395–400
24. Katz, J., Plotkin, A.: *Low-Speed Aerodynamics: From Wing Theory to Panel Methods*. Cambridge University Press (2001)